Predefined-Time Observer-Based Nonsingular Sliding-Mode Control for Spacecraft Attitude Stabilization

Jingyi Chen, Zhaoyue Chen, Haichao Zhang, *Graduate Student Member, IEEE*, Bing Xiao, *Member, IEEE*, and Lu Cao

***Abstract*—The predefined-time attitude stabilization control problem of a spacecraft with external disturbance is addressed. A predefined-time observer-based control approach is presented using a new nonsingular sliding surface. On this sliding surface, the system states can converge to zero within a predefined time. Moreover, the incorporated disturbance observer is continuous with the chattering phenomenon eliminated. Compared with the existing finite/fixed-time attitude control methods, which need a complex process to determine the settling time, the upper bound of the convergence time ensured by the presented approach is determined by a constant only. Simulation study is further given to confirm that the presented controller is effective.**

***Index Terms*—Spacecraft, attitude stabilization, sliding mode control, disturbance observer, predefined-time.**

I. Introduction

ATTITUDE stabilization is the essential maneuvering for spacecraft. Its control system design has attracted great attention with many nonlinear theory applied [1]. Among those theory, the finite-time control can stabilize the system state with finite time convergence [2]. Hence, this theory has been applied for spacecraft finite-time attitude stabilization [3]. In [4], an extended state observer-based attitude controller was designed with finite-time convergence despite actuator failure and disturbance. Although the sliding mode control associated with the Lyapunov theory is seen to design a finite/fixed-time controller, singularity will be witnessed. Although some nonsingular controllers were seen in [5], [6], the finite/fixed-time stability of the closed-loop control system can be achieved.

Manuscript received 2 September 2023; accepted 30 September 2023. Date of publication 2 October 2023; date of current version 5 March 2024. This work was supported in part by the National Natural Science Foundation of China under Grant 11972373. This brief was recommended by Associate Editor J. Ding. *(Corresponding author: Bing Xiao.)*

Jingyi Chen is with the College of Aerospace Science and Engineering, National University of Defense Technology, Changsha 410003, China (e-mail: chenjingyi256@163.com).

Zhaoyue Chen is with the Institute of Advanced Structure Technology, Beijing Institute of Technology, Beijing 100081, China (e-mail: chenzhaoyue@bit.edu.cn).

Haichao Zhang and Bing Xiao are with the School of Automation, Northwestern Polytechnical University, Xi'an 710072, China (e-mail: zhanghaichao@mail.nwpu.edu.cn; xiaobing@nwpu.edu.cn).

Lu Cao is with the National Innovation Institute of Defense Technology, Chinese Academy of Military Science, Beijing 100071, China (e-mail: caolu_space2015@163.com).

Color versions of one or more figures in this article are available at https://doi.org/10.1109/TCSII.2023.3321684.

Digital Object Identifier 10.1109/TCSII.2023.3321684

The closed-loop control system ensured by the finite/fixed-time controllers [7], [8] can achieve a fast convergence rate. However, the upper bound of the settling time needs complicated calculation. It can not be obtained by a scalar only. Therefore, the appointed-time, the predefined-time, and the prescribed-time control were presented [9], [10], [11], [12], [13]. They can stabilize that the control system within a finite-time explicitly given by the designer. In [9], an observer-based appointed-time controller was proposed for quadrotor. It was seen in [10] that the aircraft with an predefined-time attitude tracking controller could perform the necessary attitude movement within a prescribed time even in the presence of the modeling uncertainty and disturbance. Another predefined-time control method was reported in [11]. This was extended to achieve predefined-time tracking control with parametric uncertainty. Combining the prescribed performance control and the Lyapunov theory [13], an appointed-time attitude controller was designed for aircraft.To accomplish attitude maneuver of an aircraft [14], another predefined-time attitude controller was developed. Moreover, the predefined-time control was adopted to design distributed attitude coordination control for multiple spacecraft in [15]. The attitude states were governed to converge to a small region of the origin.

Motivated by the existing results of the sliding mode control and the active disturbance rejection method, a new predefined-time observer-based attitude control approach is developed in this brief. It consists of a predefined-time disturbance observer and a novel predefined-time sliding mode controller. Its main contributions are stated as follows.

1) Unlike the disturbance observers with the discontinuous signum function incorporated in [16], [17], the designed disturbance observer is continuous. The chattering phenomenon can be eliminated. Moreover, its estimation error can settle into a tiny region within a predefined time.

2) A new nonsingular sliding mode surface is presented with its sliding mode dynamic system being predefined-time stable. Then, the predefined-time controller is constructed using the disturbance observation and that sliding surface. Compared with the finite/fixed-time attitude control schemes having a complicated settling time calculation procedure in [7], [8], the upper bound of the convergence time ensured by the proposed controller is determined by only a constant.

II. Preliminaries

A. Notations

$\mathbb{R}^{m\times 1}$ and $\mathbb{R}^{m\times n}$ denote the m and the $m\times n$ dimensional Euclidean space, respectively. $\lambda_{\min}(\mathcal{M}_\delta)$ is the minimum eigenvalue of the matrix $\mathcal{M}_\delta$. sign$(\cdot)$, tanh$(\cdot)$, and arctan$(\cdot)$ are the signum, the hyperbolic tangent, and the arctangent function, respectively. $||\cdot||$ is the Euclidean norm. For any vector $\boldsymbol{x} = [x_1 \quad x_2 \quad x_3]^{\mathrm{T}} \in \mathbb{R}^{3\times 1}$, the diagnoal matrix diag$(\boldsymbol{x}) \in \mathbb{R}^{3\times 3}$ is defined with x_i as its ith principal element, $\mathbf{arctan}(\boldsymbol{x}) \in \mathbb{R}^{3\times 1}$, $\mathbf{tanh}(\boldsymbol{x}) \in \mathbb{R}^{3\times 1}$, and $\mathbf{sign}(\boldsymbol{x}) \in \mathbb{R}^{3\times 1}$ are also defined with its i element being arctan(x_i), tanh(x_i), and sign(x_i), respectively, $i = 1, 2, 3$; moreover, $\boldsymbol{x}^{\times} = [0 \quad -x_3 \quad x_2; x_3 \quad 0 \quad -x_1; -x_2 \quad x_1 \quad 0]$ is defined. $\boldsymbol{I}_n$ denotes the $n\times n$ identity matrix. $\mathbf{0}$ is the zero vector or matrix with appropriate dimension.

B. Modeling of Spacecraft Attitude Control System

The modified Rodrigues parameter $\boldsymbol{\sigma} = [\sigma_1 \quad \sigma_2 \quad \sigma_3]^{\mathrm{T}}$ is used to represent the spacecraft's attitude. Then, the kinematics and the dynamics of a rigid spacecraft are modelled as [3], [4]

$$\begin{cases} \dot{\boldsymbol{\sigma}} = \boldsymbol{G}(\boldsymbol{\sigma})\boldsymbol{\omega} \\ \boldsymbol{J}\dot{\boldsymbol{\omega}} = -\boldsymbol{\omega}^{\times}\boldsymbol{J}\boldsymbol{\omega} + \boldsymbol{\tau} + \boldsymbol{\tau}_d \end{cases} \tag{1}$$

where $\boldsymbol{\omega} = [\omega_1 \quad \omega_2 \quad \omega_3]^{\mathrm{T}}$ is the angular velocity, $\boldsymbol{J} \in \mathbb{R}^{3\times 3}$ is the inertia matrix of the spacecraft, $\boldsymbol{\tau} \in \mathbb{R}^{3\times 1}$ is the control input, $\boldsymbol{\tau}_d \in \mathbb{R}^{3\times 1}$ is the external disturbance, and $\boldsymbol{G}(\boldsymbol{\sigma}) \in \mathbb{R}^{3\times 3}$ is given as

$$\boldsymbol{G}(\boldsymbol{\sigma}) = \frac{(1-\boldsymbol{\sigma}^{\mathrm{T}}\boldsymbol{\sigma})\boldsymbol{I}_3 + 2\boldsymbol{\sigma}^{\times} + 2\boldsymbol{\sigma}\boldsymbol{\sigma}^{\mathrm{T}}}{4} \tag{2}$$

The dynamical system (1) can also be transformed into

$$\boldsymbol{M}\ddot{\boldsymbol{\sigma}} + \boldsymbol{C}(\boldsymbol{\sigma},\dot{\boldsymbol{\sigma}})\dot{\boldsymbol{\sigma}} = \boldsymbol{F}^{\mathrm{T}}\boldsymbol{\tau} + \boldsymbol{F}^{\mathrm{T}}\boldsymbol{\tau}_d \tag{3}$$

with $\boldsymbol{C}(\boldsymbol{\sigma},\dot{\boldsymbol{\sigma}}) = -\boldsymbol{F}^{\mathrm{T}}(\boldsymbol{J}\boldsymbol{F}\dot{\boldsymbol{G}} - (\boldsymbol{J}\boldsymbol{F}\dot{\boldsymbol{\sigma}})^{\times})\boldsymbol{F}$, $\boldsymbol{F} = \boldsymbol{G}^{-1}$, and $\boldsymbol{M} = \boldsymbol{F}^{\mathrm{T}}\boldsymbol{J}\boldsymbol{F}$.

Defining two new variables as $\boldsymbol{x}_1 = \boldsymbol{\sigma}$ and $\boldsymbol{x}_2 = \dot{\boldsymbol{\sigma}}$, then the system (3) can be rewritten as

$$\begin{cases} \dot{\boldsymbol{x}}_1 = \boldsymbol{x}_2 \\ \dot{\boldsymbol{x}}_2 = \boldsymbol{\Phi}\boldsymbol{x}_2 + \boldsymbol{\Psi}\boldsymbol{\tau} + \boldsymbol{d} \end{cases} \tag{4}$$

where $\boldsymbol{\Phi} = -\boldsymbol{M}^{-1}\boldsymbol{C}(\boldsymbol{x}_1, \boldsymbol{x}_2)$ and $\boldsymbol{\Psi} = \boldsymbol{M}^{-1}\boldsymbol{F}^{\mathrm{T}}$. $\boldsymbol{d} = \boldsymbol{M}^{-1}\boldsymbol{F}^{\mathrm{T}}\boldsymbol{\tau}_d$ denotes the lumped external disturbance.

Assumption 1: The lumped disturbance $\boldsymbol{d}$ in (4) is bounded by $\|\boldsymbol{d}\| \le \delta_d$, where $\delta_d > 0$ is an unknown positive constant.

It is discussed in [18] that the external disturbance $\boldsymbol{\tau}_d$ acting on any orbital spacecraft in practice is bounded by an unknown constant. Because $||\boldsymbol{M}||$ and $||\boldsymbol{F}||$ are bounded, using the definition of $\boldsymbol{d}$ can prove that $\|\boldsymbol{d}\|$ will be bounded by an unknown scalar. Assumption 1 is thus reasonable.

The control objective of this brief can be stated as: For the spacecraft attitude control system (4) with Assumption 1 satisfied, design a nonsingular sliding mode controller to achieve attitude stabilization within a predefined time. Moreover, this goal should be achieved even in the presence of external disturbance.

III. Main Results

In this part, a disturbance observer is firstly designed for the system (4). Then, the procedure for constructing the nonsingular sliding mode manifold is described. Finally, the predefined-time attitude controller design method is presented based on the designed sliding mode surface and the disturbance observation.

A. Predefined-Time Disturbance Observer

To design a predefined-time disturbance observer, a variable $\boldsymbol{\zeta} = \boldsymbol{\xi} - \boldsymbol{x}_2$ is defined. The variable $\boldsymbol{\xi}$ is updated by

$$\dot{\boldsymbol{\xi}} = \boldsymbol{\Phi}\boldsymbol{x}_2 + \boldsymbol{\Psi}\boldsymbol{\tau} + \hat{\boldsymbol{d}} \tag{5}$$

where $\hat{\boldsymbol{d}}$ is designed as

$$\hat{\boldsymbol{d}} = -\frac{\pi}{2m_1T_s}\left(L_1^{-\frac{m_1}{2}} + L_1^{\frac{m_1}{2}}\right)\boldsymbol{\zeta} - \gamma\,\mathbf{tanh}\left(\frac{\boldsymbol{\zeta}}{\varsigma}\right) \tag{6}$$

with $0 < m_1 < 1$, $\gamma > \delta_d$. ς and γ are positive constants to be selected. T_s represents the predefined time constant. $L_1 = \boldsymbol{\zeta}^{\mathrm{T}}\boldsymbol{\zeta}$ represents a Lyapunov function.

Theorem 1: Considering the attitude control system (4) and Assumption 1, a continuous disturbance observer is given as (6). The observer can achieve an accurate observation of $\boldsymbol{d}$ within a predefined time $T_{s1} = \sqrt{\kappa}T_s$ with $\kappa > 1$.

Proof: Differentiating Lyapunov function L_1 yields

$$\begin{aligned} \dot{L}_1 &= 2\boldsymbol{\zeta}^{\mathrm{T}}\left(-\frac{\pi}{2m_1T_s}\left(L_1^{-\frac{m_1}{2}} + L_1^{\frac{m_1}{2}}\right)\boldsymbol{\zeta} - \gamma\,\mathbf{tanh}\left(\frac{\boldsymbol{\zeta}}{\varsigma}\right) - \boldsymbol{d}\right) \\ &= -\frac{\pi}{m_1T_s}\left(L_1^{1-\frac{m_1}{2}} + L_1^{1+\frac{m_1}{2}}\right) - 2\gamma\boldsymbol{\zeta}^{\mathrm{T}}\mathbf{tanh}\left(\frac{\boldsymbol{\zeta}}{\varsigma}\right) - 2\boldsymbol{\zeta}^{\mathrm{T}}\boldsymbol{d} \end{aligned} \tag{7}$$

Using the inequality $|\mu| - \mu\tanh(\frac{\mu}{\epsilon}) \le \eta\epsilon$ with $\eta = 0.2785$, $\epsilon > 0$, and $\mu \in \mathbb{R}$, the following inequality always holds

$$\begin{aligned} -2\boldsymbol{\zeta}^{\mathrm{T}}\boldsymbol{d} \le 2\sum_{i=1}^{3}|\zeta_i|\gamma &\le 2\sum_{i=1}^{3}\gamma\zeta_i\tanh\left(\frac{\zeta_i}{\varsigma}\right) + 6\varsigma\gamma\eta \\ &= 2\gamma\boldsymbol{\zeta}^{\mathrm{T}}\mathbf{tanh}\left(\frac{\boldsymbol{\zeta}}{\varsigma}\right) + \vartheta \end{aligned} \tag{8}$$

with $\vartheta = 6\varsigma\gamma\eta$.

Substituting (8) into (7) results in

$$\dot{L}_1 \le -\frac{\pi}{m_1T_s}\left(L_1^{1-\frac{m_1}{2}} + L_1^{1+\frac{m_1}{2}}\right) + \vartheta \tag{9}$$

Referring to [19], it can be proved that L_1 can decrease to a small region $\mathcal{D}_1$ within predefined time $T_{s1} = \sqrt{\kappa}T_s$, where $\mathcal{D}_1$ is given by

$$\mathcal{D}_1 = \left\{L_1 \le \min\left\{\left(\frac{\kappa m_1T_{s1}\vartheta}{(\kappa-1)\pi}\right)^{\frac{2}{2-m_1}}, \left(\frac{\kappa m_1T_{s1}\vartheta}{(\kappa-1)\pi}\right)^{\frac{2}{2+m_1}}\right\}\right\} \tag{10}$$

Therefore, $\boldsymbol{\zeta}$ has an upper bound. Then the following formula can be satisfied $\lim_{t\to\infty}||\dot{\boldsymbol{\zeta}}|| = 0$. Further, on the basis of the definition of $\boldsymbol{\zeta}$, one has $\dot{\boldsymbol{\zeta}} = \hat{\boldsymbol{d}} - \boldsymbol{d} = \tilde{\boldsymbol{d}}$. The estimation error $\tilde{\boldsymbol{d}}$ stabilizes to zero asymptotically. Therefore, for all $t > T_{s1}$, there is a small constant d_a such that $||\tilde{\boldsymbol{d}}|| \le d_a$. Thereby the proof of Theorem 1 is completed.

Remark 1: The constant κ can determine the upper bound of the system's convergence time and the size of the residual set $\mathcal{D}_1$. In fact, the size of the residual set $\mathcal{D}_1$ decreases and the settling time T_{s1} increases when the parameter κ increases. In this brief, $\kappa = 2$ is selected. Hence, L_1 decreases to a small region $\mathcal{D}_2 = \left\{L_1 \leq \min\left\{\left(\frac{2m_1T_{s1}\vartheta}{\pi}\right)^{\frac{2}{2-m_1}}, \left(\frac{2m_1T_{s1}\vartheta}{\pi}\right)^{\frac{2}{2+m_1}}\right\}\right\}$, which can be regarded as the $\boldsymbol{d}$ that is estimated by the $\hat{\boldsymbol{d}}$ within a predefined time $T_{s1} = \sqrt{2}T_s$.

B. Nonsingular Predefined-Time Sliding Mode Surface

Theorem 2: Considering the control system (4), a new sliding mode surface is designed as

$$\boldsymbol{s} = (\lambda \boldsymbol{x}_2)^{p/q} + \Gamma^{p/q}(\boldsymbol{x}_1)\mathbf{arctan}(\boldsymbol{x}_1) \tag{11}$$

with $\lambda = \frac{T_{s2}(p-q)}{p(3\pi^2/4)^{(p-q)/2p}}$, $1 < p/q < 2$, and $\Gamma(\boldsymbol{x}_1) = \mathrm{diag}([(1+x_{11}^2)(1+x_{12}^2)\ (1+x_{13}^2)])$. T_{s2} is a predefined time constant. The variables $\boldsymbol{x}_1$ and $\boldsymbol{x}_2$ will stabilize to the equilibrium point within a predefined time T_{s2} when the ideal sliding mode motion starts, *i.e.,* $\boldsymbol{s} = 0$.

Proof: When $\boldsymbol{s} = \mathbf{0}$, one has

$$(\lambda \boldsymbol{x}_2)^{p/q} + \Gamma^{p/q}(\boldsymbol{x}_1)\mathbf{arctan}(\boldsymbol{x}_1) = \mathbf{0} \tag{12}$$

By an equivalent transformation, it yields

$$\lambda \boldsymbol{x}_2 + \Gamma(\boldsymbol{x}_1)(\mathbf{arctan}(\boldsymbol{x}_1))^{q/p} = \mathbf{0} \tag{13}$$

Introducing a new variable $\boldsymbol{\Xi} = \mathbf{arctan}(\boldsymbol{x}_1)$, (13) can be rewritten as

$$\lambda \dot{\boldsymbol{\Xi}} + \boldsymbol{\Xi}^{q/p} = \mathbf{0} \tag{14}$$

Choosing a positive Lyapunov function $L_2 = \boldsymbol{\Xi}^{\mathrm{T}}\boldsymbol{\Xi}$, then its time derivative of L_2 becomes

$$\dot{L}_2 = -\frac{2}{\lambda}\boldsymbol{\Xi}^{\mathrm{T}}\boldsymbol{\Xi}^{q/p} \leq -\frac{2}{\lambda}L_2^{(p+q)/2p} \tag{15}$$

According to [4, Lemma 1], the function L_2 will decrease to zero. The settling time can be computed by

$$t \leq \frac{\lambda p}{p-q}(L_2(0))^{\frac{p-q}{2p}} \leq \frac{\lambda p}{p-q}\left(\frac{3\pi^2}{4}\right)^{\frac{p-q}{2p}} = T_{s2} \tag{16}$$

with $L_2(0)$ being the initial value of L_2. Thereby the proof of Theorem 2 is completed.

Remark 2: Inspired by the results in [6], a new predefined-time nonsingular sliding mode surface (11) is developed. Once the ideal sliding mode dynamic, denoted by $\boldsymbol{s} = 0$, is established, the state $\boldsymbol{x}_1$ in (11) can converge to the origin within predefined time T_{s2}. Compared with the preceding finite/fixed-time sliding surfaces with a complicated settling time calculation procedure reported in [5], [6], the proposed sliding surface $\boldsymbol{s}$ can ensure that the system state converges to the origin along the sliding surface with a simple settling time's upper bound, *i.e.,* a positive constant.

C. Nonsingular Predefined-Time Sliding Mode Controller

Differentiate $\boldsymbol{s}$ to design the nonsingular predefined-time control scheme. Hence, one has

$$\begin{aligned}\dot{\boldsymbol{s}} = &\frac{p}{q}\lambda^{p/q}\mathrm{diag}(\boldsymbol{x}_2^{p/q-1})\dot{\boldsymbol{x}}_2 + \boldsymbol{\Upsilon} = \frac{p}{q}\lambda^{p/q}\mathrm{diag}\left(\boldsymbol{x}_2^{p/q-1}\right)\\ &\times(\boldsymbol{\Phi}\boldsymbol{x}_2 + \boldsymbol{\Psi}\boldsymbol{\tau} + \boldsymbol{d}) + \boldsymbol{\Upsilon}\end{aligned} \tag{17}$$

where $\boldsymbol{\Upsilon}$ is given as

$$\begin{cases}\boldsymbol{\Upsilon} = \frac{2p}{q}\Gamma^{p/q-1}(\boldsymbol{x}_1)\mathcal{A} + \Gamma^{p/q}(\boldsymbol{x}_1)\mathcal{B}\\ \mathcal{A} = \mathrm{diag}([x_{11}x_{21}\ \ x_{12}x_{22}\ \ x_{13}x_{23}])\mathbf{arctan}(\boldsymbol{x}_1)\\ \mathcal{B} = \left[\frac{x_{21}}{1+x_{11}^2}\ \ \frac{x_{22}}{1+x_{12}^2}\ \ \frac{x_{23}}{1+x_{13}^2}\right]^{\mathrm{T}}\end{cases} \tag{18}$$

The attitude controller is designed as $\boldsymbol{\tau} = \boldsymbol{\tau}_1 + \boldsymbol{\tau}_2$, which is given by

$$\begin{cases}\boldsymbol{\tau}_1 = \boldsymbol{\Psi}^{-1}\Big(-\hat{\boldsymbol{d}} - a_3\mathbf{sign}(\boldsymbol{s}) - \boldsymbol{\Phi}\boldsymbol{x}_2\\ \qquad -\frac{q}{p}\lambda^{-p/q}\mathrm{diag}(\boldsymbol{x}_2^{2-p/q})\Big(\Gamma(\boldsymbol{x}_1)^{p/q-1}\\ \qquad +\frac{2p}{q}\Gamma(\boldsymbol{x}_1)^{p/q-1}\mathrm{diag}(\boldsymbol{x}_1)\mathbf{arctan}(\boldsymbol{x}_1)\Big)\Big)\\ \boldsymbol{\tau}_2 = \frac{q}{p}\lambda^{-p/q}\boldsymbol{\Psi}^{-1}\mathrm{diag}\big((x_{2i})^{1-p/q}\zeta(x_{2i}^{p/q-1})\big)\\ \qquad \left(-\frac{2\boldsymbol{s}^{m_2}}{(1-m_2)T_{s3}} - \frac{2\boldsymbol{s}^{n_2}}{(n_2-1)3^{\frac{1-n_2}{2}}T_{s3}}\right)\end{cases} \tag{19}$$

with $i = 1, 2, 3$. $0 < m_2 < 1$ and $n_2 > 1$ are positive real numbers. a_3 is a positive scalar such that $a_3 > d_a$. T_{s3} is the predefined time constant. The continuous piecewise function $\zeta(\cdot)$ is defined as [5]

$$\zeta(x_{2i}^{p/q-1}) = \begin{cases}\sin\left(\frac{\pi}{2\varepsilon}x_{2i}^{p/q-1}\right), & x_{2i}^{p/q-1} \leq \varepsilon\\ 1, & x_{2i}^{p/q-1} > \varepsilon\end{cases} \tag{20}$$

where ε is a positive real number.

Theorem 3: When the predefined-time attitude controller $\boldsymbol{\tau} = \boldsymbol{\tau}_1 + \boldsymbol{\tau}_2$ given by (19) is implemented to the attitude control system (4), it can be stabilized in a predefined time.

Proof: In view of the piecewise function (20), there are the following two regions in the whole state space

$$\begin{cases}\mathscr{A}_1 = \left\{(\boldsymbol{x}_1, \boldsymbol{x}_2) \mid |x_{2i}|^{p/q-1} > \varepsilon\right\}\\ \mathscr{A}_2 = \left\{(\boldsymbol{x}_1, \boldsymbol{x}_2) \mid |x_{2i}|^{p/q-1} \leq \varepsilon\right\}\end{cases} \tag{21}$$

Next, the proof process of Theorem 3 in both regions given by (21) will be described in detail.

Selecting a positive Lyapunov function as $L_3 = \boldsymbol{s}^{\mathrm{T}}\boldsymbol{s}$ and differentiating L_3, then it yields

$$\begin{aligned}\dot{L}_3 = &2\boldsymbol{s}^{\mathrm{T}}\Big(\frac{p}{q}\lambda^{p/q}\mathrm{diag}\left(\boldsymbol{x}_2^{p/q-1}\right)(\boldsymbol{\Phi}\boldsymbol{x}_2 + \boldsymbol{\Psi}\boldsymbol{\tau} + \boldsymbol{d}) + \boldsymbol{\Upsilon}\Big)\\ = &2\boldsymbol{s}^{\mathrm{T}}\Big(\mathrm{diag}\left(\zeta(x_{2i}^{p/q-1})\right)\Big(-\frac{2\boldsymbol{s}^{m_2}}{(1-m_2)T_{s3}} - \frac{2\boldsymbol{s}^{n_2}}{(n_2-1)3^{\frac{1-n_2}{2}}T_{s3}}\Big)\\ &+\boldsymbol{\rho}(\boldsymbol{x}_2)(-\tilde{\boldsymbol{d}} - a_3\mathbf{sign}(\boldsymbol{s}))\Big)\end{aligned} \tag{22}$$

with $\boldsymbol{\rho}(\boldsymbol{x}_2) = \mathrm{diag}(\frac{p}{q}\lambda^{p/q}\boldsymbol{x}_2^{p/q-1}) \in \mathbb{R}^{3\times 3}$ being a positive definite matrix.

Case I: If the states $(\boldsymbol{x}_1, \boldsymbol{x}_2)$ are in the region $\mathscr{A}_1$, one can obtain that $\zeta(x_{2i}^{p/q-1}) = 1$. Therefore, (22) is rewritten as

$$\begin{aligned}\dot{L}_3 = &\boldsymbol{s}^{\mathrm{T}}\Big(-\frac{4\boldsymbol{s}^{m_2}}{(1-m_2)T_{s3}} - \frac{4\boldsymbol{s}^{n_2}}{(n_2-1)3^{\frac{1-n_2}{2}}T_{s3}}\\ &+\boldsymbol{\rho}(\boldsymbol{x}_2)(-\tilde{\boldsymbol{d}} - a_3\mathbf{sign}(\boldsymbol{s}))\Big)\\ \leq &-\frac{4(||\boldsymbol{s}||^2)^{\frac{m_2+1}{2}}}{(1-m_2)T_{s3}} - \frac{4(||\boldsymbol{s}||^2)^{\frac{n_2+1}{2}}}{(n_2-1)T_{s3}}\\ &+\lambda_{\min}(\boldsymbol{\rho}(\boldsymbol{x}_2))(\Delta_d - a_3)||\boldsymbol{s}||\end{aligned}$$

$$\leq -\frac{4}{(1-m_2)T_{s3}}L_3^{\frac{m_2+1}{2}} - \frac{4}{(n_2-1)T_{s3}}L_3^{\frac{n_2+1}{2}} \quad (23)$$

Referring to [7, Lemma 2], the Lyapunov function L_3 will decrease to zero. The settling time is determined by

$$t \leq \frac{(1-m_2)T_{s3}}{4}\frac{2}{1-m_2} + \frac{(n_2-1)T_{s3}}{4}\frac{2}{n_2-1} = T_{s3} \quad (24)$$

Note that $L_3 = 0$ means $\boldsymbol{s} = \boldsymbol{0}$. The system state $(\boldsymbol{x}_1, \boldsymbol{x}_2)$ can reach the sliding mode surface or be driven into the other region $\mathscr{A}_2$.

Case II: When the states $(\boldsymbol{x}_1, \boldsymbol{x}_2)$ are in the region $\mathscr{A}_2$. One can conclude that $\mathscr{A}_2$ is not an attractor except for the origin. By employing the fact $\zeta(x_{2i}^{p/q-1})x_{2i}^{1-p/q} \to \frac{\pi}{2\varepsilon}$ as $x_{2i} \to 0$, the controller $\boldsymbol{\tau} = \boldsymbol{\tau}_1 + \boldsymbol{\tau}_2$ given by (19) can be rewritten as

$$\boldsymbol{\tau} = \boldsymbol{\Psi}^{-1}\Bigg(-\hat{\boldsymbol{d}} - a_3\,\mathbf{sign}(\boldsymbol{s}) + \frac{q}{p}\lambda^{-p/q}\frac{\pi}{2\varepsilon}\Bigg(-\frac{2\boldsymbol{s}^{m_2}}{(1-m_2)T_{s3}} - \frac{2\boldsymbol{s}^{n_2}}{(n_2-1)3^{\frac{1-n_2}{2}}T_{s3}}\Bigg) - \boldsymbol{\Phi}\boldsymbol{x}_2\Bigg) \quad (25)$$

Substituting the degenerated predefined-time controller (25) into the control system (4), it yields

$$\dot{\boldsymbol{x}}_2 = -\frac{q}{p}\lambda^{-p/q}\frac{\pi}{2\varepsilon}\left(\frac{2\boldsymbol{s}^{m_2}}{(1-m_2)T_{s3}} + \frac{2\boldsymbol{s}^{n_2}}{(n_2-1)3^{\frac{1-n_2}{2}}T_{s3}}\right) + \boldsymbol{d} - \hat{\boldsymbol{d}} - a_3\,\mathbf{sign}(\boldsymbol{s}) \quad (26)$$

According to (26), using the condition $a_3 > d_a$, one can obtain that $\dot{\boldsymbol{x}}_2 < 0$ if the following inequality $\boldsymbol{s} > 0$ holds; $\dot{\boldsymbol{x}}_2 > 0$ if the inequality $\boldsymbol{s} < 0$ holds. Therefore, the state trajectory can pass through the region $\mathscr{A}_2$ into the region $\mathscr{A}_1$ within short time. Further, if the parameter ε is selected small enough, the time of crossing region $\mathscr{A}_2$ can be neglected [5], [9]. In fact, the positive constant ε can be selected very small to circumvent the singularity problem and to decrease the negligible crossing time between two regions $\mathscr{A}_1$ and $\mathscr{A}_2$. Therefore, the total settling time of the control system (4) with the application of the predefined-time controller $\boldsymbol{\tau} = \boldsymbol{\tau}_1 + \boldsymbol{\tau}_2$ given by (19) can be computed as $t \leq T_{s1} + T_{s2} + T_{s3}$. Thereby the proof of Theorem 3 is completed.

Remark 3: The idea of using continuous piecewise functions to design a nonsingular sliding mode controller is inspired by [5]. Similarly, the predefined-time sliding mode controller $\boldsymbol{\tau} = \boldsymbol{\tau}_1 + \boldsymbol{\tau}_2$ given by (19) is undefined when the variable $\boldsymbol{x}_2 = \boldsymbol{0}$. Hence, a small perturbation to the initial velocity is required in practice.

Remark 4: The discontinuous robust term $\mathbf{sign}(\boldsymbol{s})$ in (19) is employed to deal with the disturbance estimation error. Intuitively, it can cause the known control chattering phenomenon because of its non-continuity. In fact, the continuous disturbance observer (6) can compensate for the disturbances. The uncompensated disturbance only remains a very small fluctuation. At this time, we introduce a discontinuous robust term to attenuate it. The discontinuous robust term's amplitude is also very small. Therefore, the control chattering phenomenon in this brief can be weakened compared with the control scheme using discontinuous robust term to attenuate the total disturbance directly.

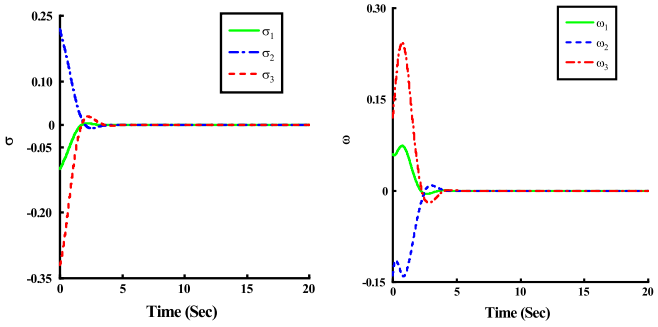

(a) Attitude MRPs (b) Angular velocity

Fig. 1. Time response curve of $\boldsymbol{\sigma}$ and $\boldsymbol{\omega}$.

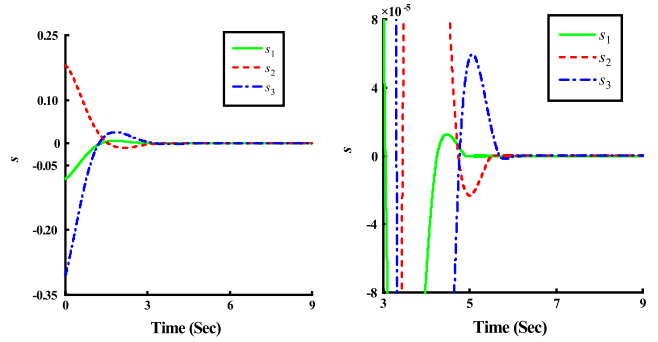

(a) Global response (b) Steady-state response

Fig. 2. Convergence performance of the sliding mode surface $\boldsymbol{s}$.

IV. Simulation Results

The simulation study of spacecraft is conducted to verify the effectiveness of the developed control scheme $\boldsymbol{\tau} = \boldsymbol{\tau}_1 + \boldsymbol{\tau}_2$ given by (19) in this section. In simulation, the inertia matrix of a spacecraft is set as $\boldsymbol{J} = [20\ \ 0\ \ 0.9; 0\ \ 17\ \ 0; 0.9\ \ 0\ \ 15]\text{kg}\cdot\text{m}^2$. The external disturbance is assumed as

$$\boldsymbol{\tau}_d = \begin{bmatrix} 4\cos(10\xi_d t) + 3\sin(3\xi_d t) - 8 \\ 6.5\cos(2\xi_d t) - 1.2\sin(4\xi_d t) + 10 \\ 5\cos(3\xi_d t) - 1.5\sin(2\xi_d t) + 15 \end{bmatrix} \times 10^{-3}\ \text{Nm} \quad (27)$$

where $\xi_d = ||\boldsymbol{\omega}|| + 0.01$. The initial states of the spacecraft are given as $\boldsymbol{\sigma}(0) = [-0.1\ \ 0.22\ \ -0.32]^{\mathrm{T}}$ and $\boldsymbol{\omega}(0) = [0.06\ \ -0.14\ \ 0.12]^{\mathrm{T}}\text{rad/s}$. The control gains in (6), (11), and (19) are selected as $T_{s1} = 5$, $T_{s2} = 5$, $T_{s3} = 10$, $p = 19$, $q = 17$, $m_1 = 0.4$, $\gamma = 0.001$, $\varsigma = 0.02$, $m_2 = 0.87$, and $n_2 = 1.5$.

With the application of the proposed control approach, the spacecraft attitude and the angular velocity convergence performance can be observed in Fig. 1(a) and Fig. 1(b), respectively. The attitude $\boldsymbol{\sigma}$ converges to a neighborhood around the origin rapidly within 10 seconds. Correspondingly, the angular velocity $\boldsymbol{\omega}$ also achieves fast convergence. The convergence accuracy of the spacecraft attitude is superior to 2×10^{-10}. The angular velocity control accuracy is better than $5 \times 10^{-8}\text{rad/s}$, *i.e.*, $||\sigma_j|| < 2 \times 10^{-10}$, $||\omega_j|| < 5 \times 10^{-8}\text{rad/s}$, with $j = 1, 2, 3$. The good convergence performance can be verified by the illustration of the sliding mode manifold in Fig. 2. It is seen the system states will reach the sliding surface after 6 seconds and stay in it thereafter. The

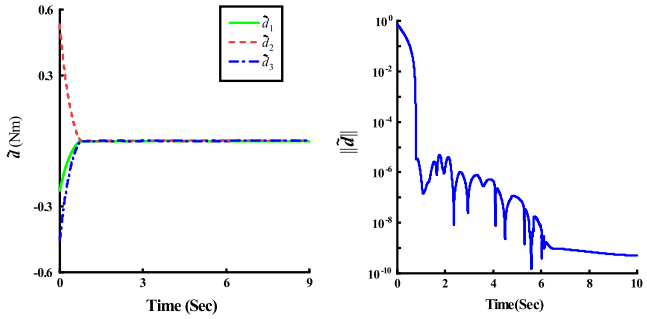

(a) Global response (b) Curve of $||\tilde{\boldsymbol{d}}||$

Fig. 3. Convergence performance of the disturbance estimation error $\tilde{\boldsymbol{d}}$.

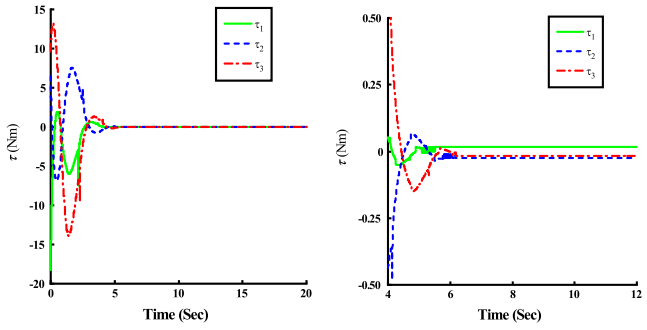

(a) Global response (b) Steady-state response

Fig. 4. Time response curve of the control input $\boldsymbol{\tau}$.

predefined-time sliding motion of the proposed sliding surface stated in Theorem 2 is therefore demonstrated.

As plotted in Fig. 3, the lumped external disturbance $\boldsymbol{d}$ in this simulation can be fast estimated. Within a predefined time, $T_{s1} = \sqrt{2} \times 5$ seconds, the estimation error is constrained to a tiny neighborhood that includes the origin. Moreover, from Fig. 3(b), it is shown that the error convergence accuracy of the observed external disturbance is greater than 1×10^{-8}, *i.e.,* $||\tilde{\boldsymbol{d}}|| \leq 1 \times 10^{-8}$. Further, the developed nonsingular predefined-time sliding mode controller to accomplish attitude maneuver is demonstrated in Fig. 4. It shows that the control chattering phenomenon can be weakened, as analyzed in Remark 4. Finally, as shown in Fig. 1 (a), the considered spacecraft's attitude movement in simulation is accomplished well within a predefined time $t \leq T_{s1} + T_{s2} + T_{s3} = \sqrt{2} \times 5 + 5 + 10$ seconds.

V. Conclusion

An observer-based predefined control scheme was presented in this brief to stabilize spacecraft attitude system. The incorporated continuous disturbance observer governed the observation error into a tiny region in a predefined time. The closed-loop attitude control system was stabilized within a predefined time despite the external disturbance. Experimental tests to verify the application capability of the proposed approach will be carried out in the future. Moreover, application of this scheme to autonomous vehicles/microsatellite or their swarm control system based on the dynamics model given in [20], [21], [22], [23] will be another future work.

References

[1] S. Xie and Q. Chen, "Adaptive nonsingular predefined-time control for attitude stabilization of rigid spacecrafts," *IEEE Trans. Circuits Syst. II, Exp. Briefs*, vol. 69, no. 1, pp. 189–193, Jan. 2022.

[2] T. Huang, J. Wang, H. Pan, and W. Sun, "Finite-time fault-tolerant integrated motion control for autonomous vehicles with prescribed performance," *IEEE Trans. Transport. Electrific.*, vol. 9, no. 3, pp. 4255–4265, Sep. 2023, doi: 10.1109/TTE.2022.3232521.

[3] H. Du and S. Li, "Finite-time attitude stabilization for a spacecraft using homogeneous method," *J. Guid. Control Dyn.*, vol. 35, no. 3, pp. 740–748, May 2012.

[4] B. Li, Q. Hu, and Y. Yang, "Continuous finite-time extended state observer based fault tolerant control for attitude stabilization," *Aerosp. Sci. Technol.*, vol. 84, pp. 204–213, Jan. 2019.

[5] Z. Zuo, "Nonsingular fixed-time consensus tracking for second-order multi-agent networks," *Automatica*, vol. 54, pp. 305–309, Apr. 2015.

[6] J. Zhai and G. Xu, "A novel non-singular terminal sliding mode trajectory tracking control for robotic manipulators," *IEEE Trans. Circuits Syst. II, Exp. Briefs*, vol. 68, no. 1, pp. 391–395, Jan. 2021.

[7] Q. Chen, S. Xie, and X. He, "Neural-network-based adaptive singularity-free fixed-time attitude tracking control for spacecrafts," *IEEE Trans. Cybern.*, vol. 51, no. 10, pp. 5032–5045, Oct. 2021.

[8] M. Zhuang, L. Tan, K. Li, and S. Song, "Fixed-time formation control for spacecraft with prescribed performance guarantee under input saturation," *Aerosp. Sci. Technol.*, vol. 119, Dec. 2021, Art. no. 107176.

[9] B. Li, W. Gong, Y. Yang, B. Xiao, and D. Ran, "Appointed fixed time observer-based sliding mode control for a quadrotor UAV under external disturbances," *IEEE Trans. Aerosp. Electron. Syst.*, vol. 58, no. 1, pp. 290–303, Feb. 2022.

[10] B. Xiao, X. Wu, L. Cao, and X. Hu, "Prescribed time attitude tracking control of spacecraft with arbitrary disturbance," *IEEE Trans. Aerosp. Electron. Syst.*, vol. 58, no. 3, pp. 2531–2540, Jun. 2022.

[11] A. J. Muñoz-Vázquez, J. D. Sánchez-Torres, E. Jiménez-Rodríguez, and A. G. Loukianov, "Predefined-time robust stabilization of robotic manipulators," *IEEE/ASME Trans. Mechatronics*, vol. 24, no. 3, pp. 1033–1040, Jun. 2019.

[12] S. Xie, Q. Chen, and X. He, "Predefined-time approximation-free attitude constraint control of rigid spacecraft," *IEEE Trans. Aerosp. Electron. Syst.*, vol. 59, no. 1, pp. 347–358, Feb. 2023.

[13] M. Liu, X. Shao, and G. Ma, "Appointed-time fault-tolerant attitude tracking control of spacecraft with double-level guaranteed performance bounds," *Aerosp. Sci. Technol.*, vol. 92, pp. 337–346, Sep. 2019.

[14] D. Ye, A.-M. Zou, and Z. Sun, "Predefined-time predefined-bounded attitude tracking control for rigid spacecraft," *IEEE Trans. Aerosp. Electron. Syst.*, vol. 58, no. 1, pp. 464–472, Feb. 2022.

[15] H.-J. Sun, Y.-Y. Wu, and J. Zhang, "A distributed predefined-time attitude coordination control scheme for multiple rigid spacecraft," *Aerosp. Sci. Technol.*, vol. 133, Feb. 2023, Art. no. 108134.

[16] M. Chen, Q. Wu, and R. Cui, "Terminal sliding mode tracking control for a class of SISO uncertain nonlinear systems," *ISA Trans.*, vol. 52, no. 2, pp. 198–206, Mar. 2013.

[17] B. Xiao, S. Yin, and H. Gao, "Reconfigurable tolerant control of uncertain mechanical systems with actuator faults: A sliding mode observer-based approach," *IEEE Trans. Control Syst. Technol.*, vol. 26, no. 4, pp. 1249–1258, Jul. 2018.

[18] B. Xiao, Q. Hu, and Y. Zhang, "Adaptive sliding mode fault tolerant attitude tracking control for flexible spacecraft under actuator saturation," *IEEE Trans. Control Syst. Technol.*, vol. 20, no. 6, pp. 1605–11612, Nov. 2012.

[19] Y. Wang, H. Wang, Y. Liu, J. Chen, T. Wu, and W. Zheng, "Modeling and predefined-time anti-disturbance control for the aerial refueling phase of receiver aircraft," *Appl. Math. Model.*, vol. 112, pp. 540–559, Dec. 2022.

[20] T. Huang, J. Wang, and H. Pan, "Adaptive bioinspired preview suspension control with constrained velocity planning for autonomous vehicles," *IEEE Trans. Intell. Veh.*, vol. 8, no. 7, pp. 3925–3935, Jul. 2023.

[21] T. Huang, H. Pan, W. Sun, and H. Gao, "Sine resistance network-based motion planning approach for autonomous electric vehicles in dynamic environments," *IEEE Trans. Transport. Electrific.*, vol. 8, no. 2, pp. 3925–3935, Jun. 2022.

[22] B. Yang, H. Huang, and L. Cao, "Centered error entropy-based sigma-point Kalman filter for spacecraft state estimation with non-Gaussian noise," *Space Sci. Technol.*, vol. 2022, Jul. 2022, Art. no. 9854601.

[23] X. Wu, B. Xiao, C. Wu, and Y. Guo, "Centroidal Voronoi tessellation and model predictive control-based macro-micro trajectory optimization of microsatellite swarm," *Space Sci. Technol.*, vol. 2022, Aug. 2022, Art. no. 9802195.